ACCSCIENCE PUBLISHING

Materials Science in Additive Manufacturing

ORIGINAL RESEARCH ARTICLE

Additively manufactured polymer punches for deep drawing: Influence of fiber deposition strategy on tool performance

Luca Giorleo[1]*, Davide Battini[2], Andrea Avanzini[2], and Elisabetta Ceretti[1]

[1]Advanced Prototyping Laboratory, Department of Mechanical and Industrial Engineering, University of Brescia, Brescia, Italy

[2]Department of Mechanical and Industrial Engineering, University of Brescia, Brescia, Italy

Abstract

Additively manufactured composite tools are increasingly used in sheet forming, yet the influence of fiber orientation on tool durability remains poorly understood. In this context, the present study investigates the limited understanding of how different continuous-fiber deposition strategies affect the mechanical stability and durability of additively manufactured polymer punches for deep drawing. Polymer tools reinforced with continuous carbon fibers were fabricated using continuous fiber fabrication (CFF) with two reinforcement layouts—concentric and isotropic—and tested until fracture to assess the achievable drawing depth, punch deformation, and cup integrity. Failure onset was monitored and the dimensional stability of the produced cups was evaluated as indicators of tool performance. The results demonstrated that fiber reinforcement increased the maximum drawable depth from 15 mm (unreinforced onyx punch) to 18 mm for concentric and 19 mm for isotropic punches. Finite element simulations reproduced the deformation trends observed experimentally, confirming that concentric reinforcement leads to higher axial compression and radial expansion. The findings highlight the potential of CFF for producing lightweight, low-cost forming tools, underscoring that optimizing fiber orientation is critical for improving tool durability and process repeatability.

Keywords: Additive manufacturing; Continuous fiber fabrication; Rapid tooling; Deep drawing; Carbon fiber reinforced polymer

***Corresponding author:**
Luca Giorleo
(luca.giorleo@unibs.it)

Citation: Giorleo L, Battini D, Avanzini A, Ceretti E. Additively manufactured polymer punches for deep drawing: Influence of fiber deposition strategy on tool performance. *Mater Sci Add Manuf.* 2026;5(2):025430101. doi: 10.36922/MSAM025430101

Received: October 26, 2025

1st revised: November 26, 2025

2nd revised: December 3, 2025

Accepted: December 3, 2025

Published online: January 14, 2026

1. Introduction

The increasing demand for flexible and cost-efficient manufacturing has encouraged the development of alternative tooling solutions capable of reducing lead time and material waste compared with conventional metallic dies. In traditional sheet metal forming, tooling typically accounts for a significant portion of production costs and time, particularly during the design and prototyping phases, where multiple die iterations are required to achieve the final geometry.[1,2] Consequently, industries with frequent design changes—such as automotive prototyping, aerospace components, and biomedical devices—are increasingly exploring non-metallic or hybrid tool materials as viable substitutes for steel or aluminum dies.[3,4]

The pursuit of agile and sustainable production has led to the widespread adoption of rapid tooling (RT) as a bridge between prototyping and manufacturing. RT uses additive manufacturing (AM) to fabricate mold inserts or forming tools directly from computer-aided design (CAD) data, significantly shortening production time and reducing costs compared to conventional machining.[1-3] Advances in AM processes, such as fused deposition modeling, selective laser sintering, and stereolithography have expanded the scope of RT from prototyping to functional short-run tooling, thereby enabling complex geometries, rapid design iterations, and local reinforcement control.[5-7]

Polymeric and composite materials are increasingly explored for RT applications due to their low cost, fast processability, and ease of customization. Fused deposition modeling, in particular, allows direct fabrication of mold inserts with tailored infill density, layer orientation, and post-processing strategies to enhance mechanical strength, thermal stability, and wear resistance.[5] Hybrid approaches, such as metal–epoxy composites, have also shown potential for improving compressive strength, thermal conductivity, and dimensional accuracy, thereby extending tool life in injection molding and forming operations.[6] Recent comparative studies between polymer- and metal-based molds demonstrate that rapid polymer tooling can achieve mechanical performance within 5–10% of aluminum tools, while offering energy savings of up to 20% per cycle and drastically reduced manufacturing time.[7] Such benefits make RT particularly attractive for micro-injection molding, sheet forming, and biomedical device prototyping, where low to medium production volumes justify the trade-off between cost and durability. In summary, the convergence of composite material development and additive-based RT is reshaping the landscape of manufacturing tools. The main challenge remains in optimizing material formulation, process parameters, and reinforcement architecture to ensure dimensional stability, surface quality, and thermal performance comparable with traditional metallic dies.[8]

In recent years, the use of additively manufactured polymer and composite tools has gained increasing attention as a viable solution for low-volume or customized forming applications.[9-14] Advances in fused filament fabrication and continuous fiber fabrication (CFF) have enabled the production of polymer-based tools with mechanical properties sufficient for moderate forming loads, while maintaining the intrinsic advantages of AM—low cost, short production time, and design flexibility.[9,14] These tools have been successfully employed in deep drawing, hydroforming, thermoforming, and die prototyping, as demonstrated in both experimental and industrial studies.[15,16] Among printable materials, onyx—a polyamide six matrix filled with chopped carbon fibers—has been widely investigated for its high stiffness-to-weight ratio and superior surface finish. When combined with continuous carbon fiber reinforcement, as in CFF printing, the resulting hybrid structures exhibit significantly enhanced compressive and flexural strength, making them suitable for punches and dies used in small-batch metal forming.[17,18] Compared with metallic tools, polymer-based tools can reduce fabrication time by up to 90% and reduce weight by 70–80%, facilitating handling and replacement.[19,20] However, despite these advantages, several limitations have been reported. The thermal and mechanical stability of polymers remains lower than that of metals, restricting their use to low-temperature and low-load processes. Wear resistance and dimensional accuracy also degrade over repeated cycles due to creep, local yielding, or surface abrasion.[12,21] Moreover, the anisotropic behavior introduced by the layer-by-layer deposition and fiber orientation strategy significantly affects tool stiffness and deformation under load.[9] These challenges have motivated numerous studies combining experimental testing and finite element modeling to better understand deformation mechanisms and predict tool performance under forming conditions.[22]

Overall, polymer and composite tools produced by AM represent a promising alternative for rapid, lightweight, and cost-effective forming solutions, particularly in prototyping or low-series production. However, the literature highlights the need for further optimization of fiber deposition strategies, enhancement of anisotropic material modeling, and validation of durability to extend their industrial applicability beyond pilot-scale use. The present study aims to evaluate the effect of fiber deposition strategy on the mechanical performance and dimensional stability of CFF-manufactured polymer punches used in deep drawing of stainless steel sheets. Two reinforcement layouts—isotropic and concentric carbon fiber deposition—were compared, and their effects on achievable drawing depth, cup geometry, and punch deformation were experimentally assessed. Furthermore, finite element simulations were performed using Deform 2D to validate experimental findings and provide insights into stress–strain distribution within the composite punches. The combined experimental and numerical approaches provide a new understanding of how fiber orientation affects tool performance, offering practical guidelines for the design of additively manufactured forming tools.

2. Materials and methods

To investigate the effect of fiber deposition strategy on the mechanical behavior and dimensional stability of polymer

punches during the deep drawing process, a combined experimental and numerical approach was adopted. This section describes the fabrication of the composite punches using CFF technology, the experimental setup employed for the deep drawing tests, the dimensional and statistical analyses performed on the formed cups, and the finite element model (FEM) developed to simulate the process and interpret the observed phenomena.

2.1. Fabrication of the polymer punches

The punches were fabricated using fused filament fabrication technology with a Markforged Mark Two printer (Markforged, United States [USA]). The layer thickness was set to 0.125 mm, resulting in a total of 320 layers. Previous studies have demonstrated that polymer-based punches subjected to compressive loading tend to experience radial displacement, which may lead to sheet clamping against the die, restricted material flow, and eventually crack initiation and cup failure.[23] To limit this deformation, continuous carbon fibers were incorporated within the onyx polymer matrix. Both the onyx filament and the continuous carbon fiber reinforcement are standard commercial materials supplied directly by Markforged, USA.[24] To ensure fiber reinforcement up to at least 20 mm from the punch top—corresponding to the maximum target cup depth—160 fiber-reinforced layers were deposited. Figure 1A illustrates the punch geometry, highlighting the onyx matrix reinforced with continuous carbon fibers embedded in an epoxy binder to allow extrusion.

Two different fiber deposition strategies were adopted: Concentric and isotropic. In the concentric strategy, continuous fibers are deposited along the external contour of each layer, forming concentric rings around the punch geometry (Figure 1B). In the isotropic strategy, fibers were oriented in multiple directions (0°, 45°, −45°, 90°) on each layer, providing nearly uniform in-plane stiffness. This pattern does not follow the part contour but instead forms a regular directional layout (Figure 1C). The onyx-only layers were printed with full-density infill and alternating raster orientations of ±45°, with a wall thickness of 2 mm for both punches. Printing parameters included a 0.4 mm brass nozzle and extrusion temperatures of 275°C for onyx and 230°C for the fiber, with the punch positioned on the build plate such that its axis was aligned with the printer's z-axis.

2.2. Deep drawing experiments

Figure 2 shows the assembly of the punch, die, and blank holder used in the experimental campaign. The deep drawing process was carried out using circular blanks with a thickness of 1 mm and a diameter of 85 mm, resulting in a drawing ratio of 2.2 (the punch diameter being 39 mm).

Regarding the drawing depth, the following procedure was adopted: In a previous study, researchers tested polymer punches made entirely of onyx and found that the maximum achievable drawing depth without failure was 15 mm.[24] Based on that study, sequential tests were conducted starting from 15 mm and increasing the depth in 1-mm increments until the maximum drawable height was reached. For each depth level, six cups were produced. The cups formed at the limiting depth—beyond which fractures occurred—were subsequently measured to evaluate the performance of the different punch configurations. Regarding the materials used, the cups were made of AISI 304 stainless steel, while the die and blank holder were manufactured from 45NiCrMo16 steel alloy. The punches were fabricated from onyx, a commercial polyamide-6-based polymer reinforced with chopped carbon fibers, and further strengthened with continuous carbon fiber reinforcement. The main mechanical properties of the materials used are summarized in Table 1.

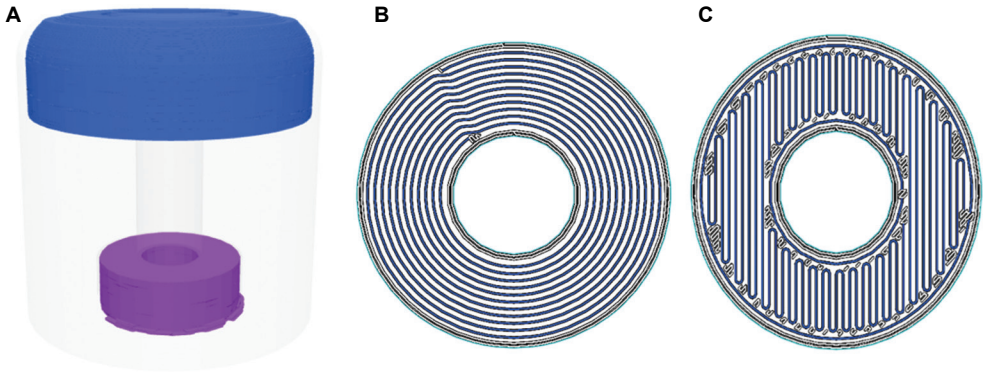

Figure 1. Geometry of the polymer punches produced through continuous fiber fabrication: (A) Overall punch model with reinforced region (blue) and support material (purple); (B) concentric fiber deposition forming circular rings; and (C) isotropic fiber deposition with alternating orientations (0° in the image)

Table 1. Mechanical properties of tools and blank material

Property	Onyx	Carbon fiber	45NiCrMo16	AISI 304
Tensile modulus (GPa)	2.4	60	284	193
Tensile stress at yield (MPa)	37	-	696	190
Tensile stress at break (MPa)	40	800	950	500–70
Tensile strain at break (%)	25	1.5	11	40
Density (g/cm^3)	1.2	1.4	7.84	8

Source: Refs. 25 and 26.

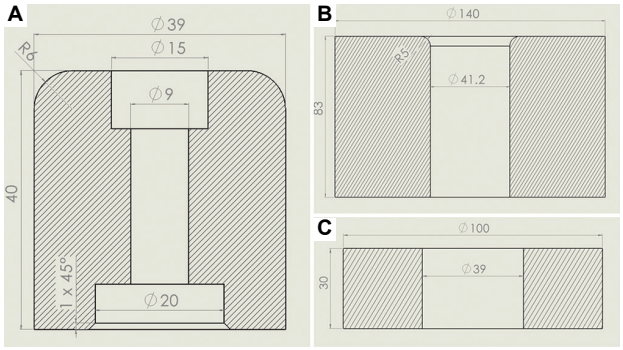

Figure 2. Geometry and dimensions of the deep drawing tooling system: (A) punch, (B) die, and (C) blank holder

The deep drawing tests were performed using a Galdabini EVL/400-A universal testing machine (Galdabini, Italy). The punch was mounted on the lower plate of the press using a threaded connection within a hollow cylindrical holder. The blank holder was fixed on the upper side of the cylinder, with the sheet blank positioned above it, while the die was attached to the upper plate of the press. The clearance between punch and die was set to 1.1 mm. After preliminary trials, a 0.1-mm gap between the blank and the blank holder was selected; this configuration ensured the correct alignment without applying a direct clamping force on the sheet. The punch velocity during forming was maintained at 10 mm/s.

2.3. Dimensional analysis

After completing the experiments, the first and sixth cups produced at the maximum achievable drawing depth were selected for dimensional analysis. Specifically, the internal circumference of each cup was measured at a height of 10 mm from the bottom, together with the longitudinal profile. From these data, the cup radius, drawing depth, and fillet radius were derived. The fillet region was evaluated using the parameter Δ_{CAD}, defined as the difference between the experimental longitudinal coordinate (x) and the nominal CAD value. Since previous studies demonstrated that the punch undergoes compressive deformation, resulting in z-direction flattening and x–y expansion,[15] the Δ_{CAD} parameter was introduced to quantify the radial enlargement of the fillet in the x–y plane.

A similar approach was adopted for the quantitative analysis of the punches. The circumference was measured at 7 mm and 15 mm from the punch base (in contact with the sheet) to determine the radius, and the longitudinal profile was acquired to evaluate punch height and fillet radius. The dimensional measurements were performed using a Renishaw Cyclone 2 coordinate measuring machine (CMM; Renishaw, United Kingdom) operating in scanning mode, with a probing resolution of 2 μm and a repeatability of ±5 μm. Each profile was acquired along a continuous circumferential path to ensure consistent point density and minimize interpolation errors. In addition, the fillet zone of each punch was scanned using a Mitaka PF60 laser probe (Mitaka, Japan) to assess the surface roughness (Ra) before and after the forming process.

The measurements obtained from the cups were analyzed as a function of both the cup production order (first or sixth) and the punch type (isotropic or concentric). For the punches, the data were analyzed as a function of either the measurement height (7 or 15 mm) or the processing stage (before or after forming). Analysis of variance was performed to assess the significance of the investigated parameters, followed by Tukey's pairwise comparison test to identify significant differences among levels (Minitab, 21.1, Minitab LLC, USA).

2.4. FEM setup and validation

The finite element simulations were performed using Deform 2D (Scientific Forming Technologies Corporation, USA), a commercial finite element software specifically designed for metal forming and large-deformation processes. The software employs an implicit Lagrangian formulation with automatic remeshing to handle severe plastic deformation, making it particularly suitable for modeling punch–sheet interaction in deep drawing operations. Axisymmetric conditions were set to reduce computational time. The die and blank holder were modeled as rigid bodies, while the punch and sheet blank were considered plastically deformable bodies. The punch was divided into two regions—upper and lower—corresponding to an unreinforced onyx punch and an onyx filled with carbon fiber, respectively, which were bonded together by a sticking condition. The geometry of the tools matched the experimental setup, except for the punch, which was modeled as a solid body, omitting the internal screw cavity. The punch velocity was set to 10 mm/s.

Both the sheet and the punch were meshed with quadrilateral elements, totaling approximately 1,000 elements per body, with a minimum element edge length of 0.15 mm. This meshing strategy was selected based on mesh-sensitivity analyses performed in our previous work on polymer punches for deep drawing,[23] where a finer discretization did not produce appreciable differences in predicted forming forces or displacement fields. A similar verification was conducted in the present study, confirming that further mesh refinement changed the radial and axial displacements by <3%. The selected element density, therefore, ensured numerically stable and accurate results while maintaining reasonable computational time. A shear friction coefficient of 0.1 was assigned to the tool–sheet interfaces, in agreement with previous studies on reinforced nylon under dry and lubricated conditions.[27,28] The simulation time was discretized using a step size of 0.1 s, and a sticking condition was also applied at the interface between the upper punch and the press to simulate the mechanical joint. Figure 3 shows the overall simulation setup.

In this study, matrix and fiber damage were not explicitly modeled because the experimental evidence showed no signs of delamination or fiber–matrix failure within the investigated load range, and the punches failed only after global deformation rather than through local damage mechanisms. Since the purpose of the FEM model was to reproduce the overall stiffness and deformation trends rather than predict fracture initiation, an elastic–plastic material law was considered sufficient and provided excellent agreement with the experimental results.

To define the constitutive laws used in the simulations, compression tests were first conducted to characterize the mechanical behavior of the printed materials. Three types of cylindrical specimens were produced: One made of an unreinforced onyx punch, one fully reinforced with concentric carbon fibers, and one with isotropic fiber reinforcement. For each configuration, three replicas were manufactured using the same process parameters (e.g., layer thickness, build orientation, reinforcement direction, extrusion temperature, and print speed) that were adopted for the punch fabrication. Following ASTM D695, the cylinders had a height of 18 mm and a diameter of 15 mm. The tests were performed using an Instron 8501 servo-hydraulic testing machine (Instron, USA) operating under displacement control at a speed of 1 mm/min. The specimens were compressed between lubricated steel plates until macroscopic failure occurred, and the nominal stresses and strains were computed from the load cell and extensometer signals. The resulting σ–ε curves were then implemented in the FEM model.

After the simulations, the axial and radial coordinates of the drawn cups were exported and compared with the experimental measurements to validate the model accuracy. Once validated, the FEM model was used to analyze the forming forces, energy consumption, and punch deformations, providing a deeper understanding of the mechanisms observed during the experiments.

3. Results

This section presents the results obtained from the experimental analysis and the corresponding statistical analyses performed on the maximum drawing height achieved before the occurrence of fracture. Table 2 summarizes the outcomes for punches made entirely of polymer (onyx) and for those reinforced with 160 layers of carbon fiber arranged either isotropically or concentrically, as illustrated in Figure 1. The results show that unreinforced

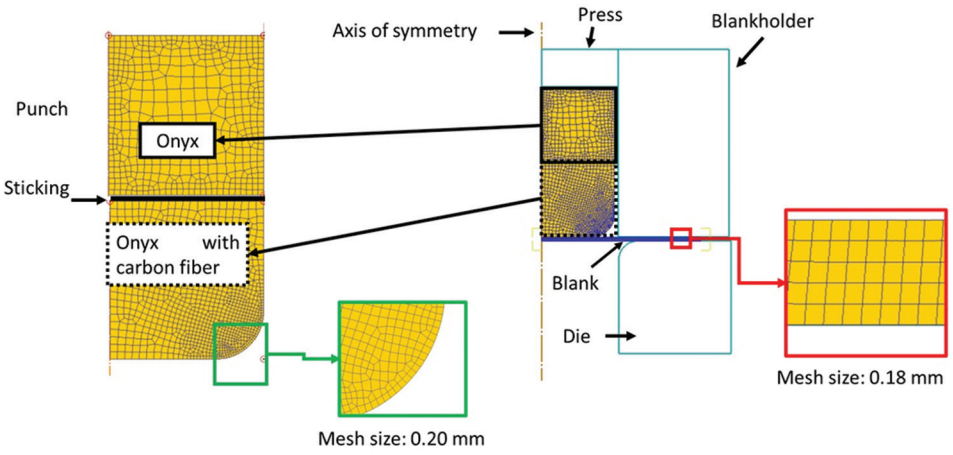

Figure 3. Finite element model setup of the deep drawing process simulated in Deform 2D under axisymmetric conditions

onyx punches were unable to produce cups with a drawing depth >15 mm. Conversely, the addition of carbon fiber significantly improved performance, allowing drawing depths up to 18 mm for the concentric configuration and up to 19 mm for the isotropic configuration. This superior performance of the isotropic configuration can be attributed to its more uniform in-plane stiffness, which distributes the compressive load more evenly throughout the punch and delays the onset of local deformation and fracture.

The representative images of the forming process and the corresponding failures are shown in Figure 4. As observed, all fractures initiated along the lateral wall of the cup and propagated tangentially toward the dome region, indicating a tensile-dominated failure mode caused by excessive thinning in the wall during the final stages of deformation. The absence of typical defects, such as wrinkling confirms that the blank-holder force and alignment conditions were properly adjusted.

Since the cups produced with the isotropic punch at a drawing height of 19 mm exhibited inconsistent results—some being successfully formed while others showed defects—these samples were excluded from further analysis. The subsequent quantitative evaluation was therefore conducted by comparing cups produced with isotropic and concentric punches at a drawing depth of 18 mm.

3.1. Cup analysis

This subsection reports the statistical analyses of the cup radius, drawing depth, and fillet radius measured using a CMM. Figure 5 displays the results for the cup radius analysis. The findings reveal that both the punch type (isotropic or concentric) and the cup production order (first or sixth cup) significantly affected the measured radius. Specifically, the results show that the cup radius tends to decrease as more cups are produced, and that concentric punches generally produce cups with larger diameters compared with isotropic punches, as confirmed by both the interval plot and Tukey's pairwise comparison test. These trends suggest a progressive deformation of the punch during repeated forming operations.

Table 2. Summary of deep drawing outcomes for polymer-only and fiber-reinforced punches at different drawing depths

Test	15 mm	16 mm	17 mm	18 mm	19 mm	20 mm
Onyx	✓	–	–	–	–	–
CC	✓	✓	✓	✓	–	–
ISO	✓	✓	✓	✓	✓	–

Notes: ✓=Drawing completed without failure; –=Drawing failure.
Abbreviations: CC: Concentric configuration; ISO: Isotropic configuration.

It should be noted that, although statistically significant, these differences are in the order of a few hundredths of a millimeter. When compared with the nominal CAD geometry, as shown in Figure 6, the experimental profiles overlap and are all slightly above the ideal CAD curve. Therefore, regardless of the punch type used, the process consistently produces cups with a diameter approximately 0.5 mm larger than the designed CAD value.

Conversely, regarding the drawing depth achieved at the end of the process, variations on the order of tenths of a millimeter were observed, as shown in the interval plot in Figure 7. In this case, the findings reveal a stronger significance for the punch type, as indicated by the corresponding *F*-values, *p*-values, and the results of Tukey's test, which identified three distinct groups. Both concentric cups were classified within group A, whereas the isotropic punch showed a differentiation between the first and sixth cups, indicating a decreasing trend in drawing depth with increasing production cycles. It should be noted that, since the depth values are negative, higher values correspond to shallower cups.

A similar observation can be made for the fillet radius, expressed by the parameter Δ_{CAD}, defined as the radial difference between the nominal CAD value and the experimental measurement. Since all Δ_{CAD} values are positive, the experimental cups exhibited smaller fillet radii than the ideal geometry. The findings reveal that the interaction effect was not significant, while both the punch type and the number of cups produced were significant. Tukey's test indicated that only the CON_06 level was significantly lower than the others.

The variation in the fillet profiles of the produced cups is shown in Figure 8. To facilitate comparison, the CAD

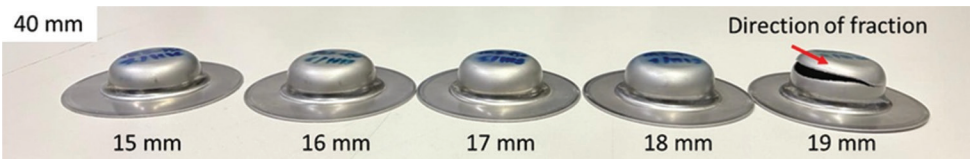

Figure 4. Representative images of deep drawing tests showing cup formation and fracture locations along the lateral wall

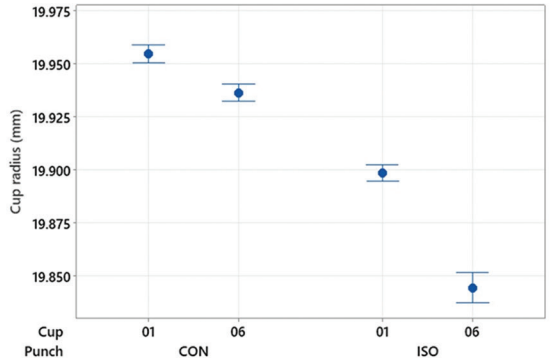

Source	DF	Adj SS	Adj MS	*F*-value	*p*-value
Cup	1	0.4260	0.42603	204.66	0.000
Punch	1	1.7789	1.77885	854.55	0.000
Cup*Punch	1	0.1036	0.10359	49.76	0.000
Error	1,292	2.6895	0.00208		
Total	1,295	4.9979			

Cup*Punch	N	Mean	Grouping
01 CON	324	19.9546	A
06 CON	324	19.9363	B
01 ISO	324	19.8984	C
06 ISO	324	19.8443	D

Figure 5. Statistical analysis of cup radius: Interval plot results (left) and Analysis of variance table with Tukey grouping (right) indicating statistically significant differences among punch configurations
Abbreviations: Adj MS: Adjusted mean square; Adj SS: Adjusted sum of squares; CON: Concentric; DF: Degrees of freedom; ISO: Isotropic

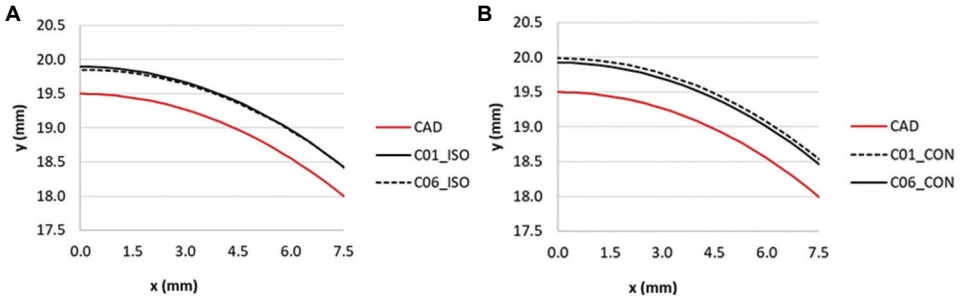

Figure 6. Comparison between experimental and nominal CAD profiles of the drawn cups: (A) ISO and (B) CON fiber deposition
Abbreviations: CAD: Computer-aided design; CON: Concentric; ISO: Isotropic

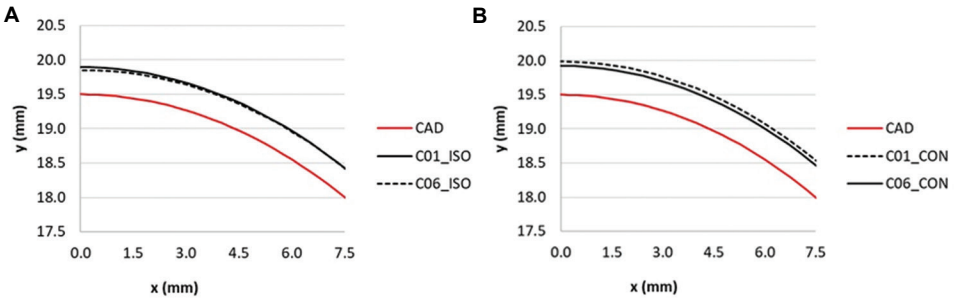

Figure 7. Statistical analysis of (A) drawing depth and (B) Δ_{CAD} values: Interval plot results (left) and Analysis of variance table with Tukey grouping (right) indicating significant differences among configurations
Abbreviations: Adj MS: Adjusted mean square; Adj SS: Adjusted sum of squares; CAD: Computer-aided design; CON: Concentric; DF: Degrees of freedom; ISO: Isotropic

curve was shifted by a consistent offset to compensate for the reduction in drawing depth measured in Figure 7. This adjustment allows a clear illustration of the actual loss of accuracy in the fillet radius relative to the ideal CAD profile (Figure 8), without the influence of the overall depth deviation observed in the previous analysis.

These findings demonstrate that punches with an isotropic fiber filling strategy produced cups with radii closer to the nominal CAD values, achieved greater drawing depths, and exhibited higher accuracy in the fillet radius compared with cups formed using concentric punches. Conversely, increasing the number of forming cycles did not lead to substantial variations in the cup radius. The drawing depth remained nearly constant for concentric punches, while a progressive reduction was observed for the isotropic configuration. Regarding the fillet radius, the cup production order (first versus sixth cup) proved to be an insignificant factor (within the levels tested in this

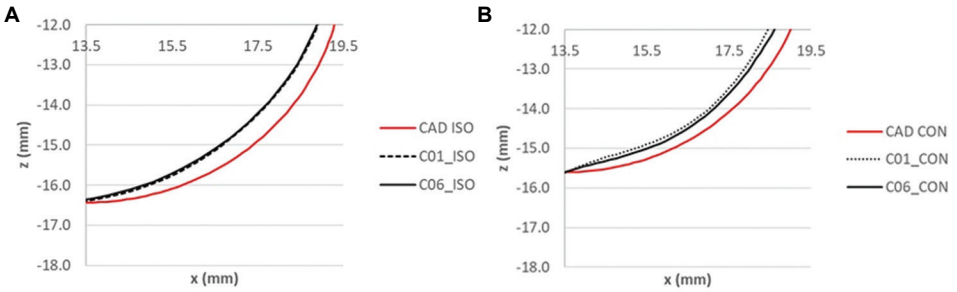

Figure 8. Comparison of experimental and CAD fillet radii for (A) ISO punch and (B) CON punch
Abbreviations: CAD: Computer-aided design; CON: Concentric; ISO: Isotropic

study) for isotropic punches, whereas concentric punches showed a slight improvement in approaching the ideal geometry.

3.2. Punch analysis

Regarding the punch analysis, a preliminary visual inspection revealed deformation of the tool in the region composed solely of polymer material, as shown in Figure 9. No permanent defects, such as cracks or delamination, were detected on the punches after the forming process. The surface finish, and particularly the characteristic stair-stepping effect typical of AM, appeared to be reduced. By contrast, an enlargement of the upper part of the punch was observed in the region made of unreinforced onyx punch.

The analysis of the punch diameter variation measured at 7 mm and 15 mm from the surface, as a function of the different fiber-filling strategies, is presented in Figure 10. Considering the nominal radius of 19.5 mm, two main phenomena can be identified. First, in the regions near the fillet radius—where stress concentration is highest—localized wear of the tool occurred, resulting in a reduction of the punch radius. Second, in the areas near the material transition zone (unreinforced onyx punch), a diametral expansion was observed due to punch compression, leading to a slight increase in diameter. Statistical analysis revealed that both the measurement height and the punch type significantly affected the measured radius, and Tukey's test indicated that the concentric strategy resulted in greater axial deformation and higher wear levels.

The increase in punch diameter can also be observed in Figure 11A, where a portion of the circumference acquired by the CMM is reported for the four measurement points. Figure 11B, which displays the cross-sectional profile of the punch area in contact with the sheet and the fillet radius, highlights the compression experienced by the punches compared with the nominal CAD surface. This deformation resulted in final punch heights of 39.4 mm for the concentric configuration and 39.6 mm for the isotropic configuration. Figure 11B also illustrates the wear phenomenon, which caused a reduction in the punch fillet profile relative to the original geometry.

To further support the observed wear phenomenon, Figures 12 and 13 present the analysis of the average surface roughness (Ra) measured before (pre) and after (post) the forming process. Statistical analysis revealed that the only statistically significant factor was the processing condition, which caused an average reduction in surface roughness from 28.8 ± 2.4 μm to 13.2 ± 3.1 μm. Figure 13 also shows that the surface finish became smoother, with a less varied color range, and that the typical stair-stepping effect of additively manufactured parts was significantly reduced after the forming operation. It is important to note that the stair-stepping effect observed on the punch surface is purely geometric and did not induce any form of delamination under the test conditions. Post-forming inspections revealed no interlayer separation, confirming that the CFF process provides adequate bonding between layers and prevents structural degradation under the tested loading conditions.

These findings demonstrate that, during the forming of stainless-steel cups, the tools experienced compression-induced flattening. This deformation resulted in an increased radius in the regions without fiber reinforcement, a reduction in punch height, and variations in both the fillet radius and surface finish due to wear. The influence of the fiber-filling strategy was evident: Concentric fiber deposition led to a greater reduction in punch height, a larger diametral expansion measured at 15 mm from the top surface, and more pronounced wear compared with the isotropic configuration. These experimental observations on punch deformation and wear were further analyzed through finite element simulations to clarify the stress distribution and deformation mechanisms.

4. FEM analysis

This section presents the results of the deep drawing simulations performed using the two different punches

manufactured with concentric and isotropic fiber deposition strategies. As discussed in Section 2, compression tests were carried out on cylindrical specimens fabricated according to rectangular specimens (10 × 10 × 10 mm) to characterize the material law used as input for the Deform 2D software. Figure 14 shows the compression test results together with the statistical analysis of a cubic regression model used to describe the stress–strain relationship (σ–ε). As observed, in all cases, the constant, linear, quadratic, and cubic terms were statistically significant (p<0.001). Furthermore, the lack-of-fit test returned a value of 1 for all models, indicating an excellent fit to the experimental data. The coefficients of the regression equations used to simulate the behavior of unreinforced onyx punch and onyx reinforced with isotropic or concentric carbon fibers are reported in Table 3.

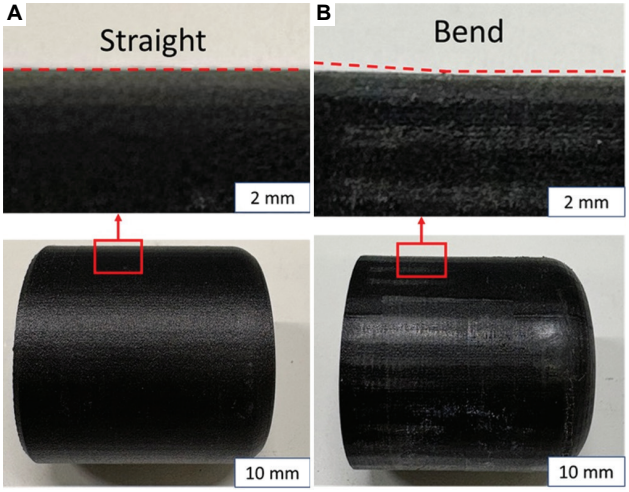

Figure 9. Polymer punches (A) before and (B) after deep drawing, showing deformation in the unreinforced polymer region and no visible cracks or delamination

Once the simulations were completed, the model accuracy was first validated by comparing the simulated cup geometry with the experimental results for both punch configurations, as shown in Figure 15. The FEM model accurately reproduced the experimental outcomes, with deviations within a few tenths of a millimeter. Therefore, the validated FEM model was subsequently used to evaluate possible differences in forming forces and energy consumption, as well as to estimate the punch deformations and explain the experimental findings.

Figure 16 displays the plots of axial force and forming energy as a function of the punch stroke. The findings reveal that no significant differences were detected between the two punch configurations. However, the

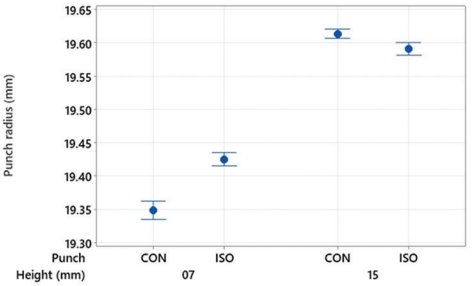

Source	DF	Adj SS	Adj MS	*F*-value	*p*-value
Height	1	15.0685	15.0685	1,702.67	0.000
Punch	1	0.2383	0.2383	26.93	0.000
Height *Punch	1	0.7960	0.7960	89.94	0.000
Error	1,304	11.5403	0.0088		
Total	1,307	27.6430			

Height*Punch	N	Mean	Grouping
15 CON	327	19.6130	A
15 ISO	327	19.5906	B
07 ISO	327	19.4253	C
07 CON	327	19.3490	D

Figure 10. Statistical analysis of punch radius: Interval plot results (left) and Analysis of variance table and Tukey grouping (right) indicating significant differences among configurations
Abbreviations: Adj MS: Adjusted mean square; Adj SS: Adjusted sum of squares; CON: Concentric; DF: Degrees of freedom; ISO: Isotropic

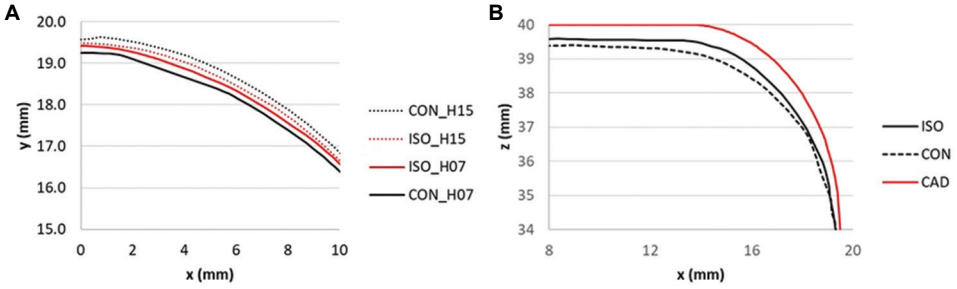

Figure 11. Comparison of nominal and deformed punch geometry: (A) Circumferential section acquired by coordinate measuring machine; (B) longitudinal profile highlighting compression and wear near the fillet
Abbreviations: CAD: Computer-aided design; CON: Concentric; ISO: Isotropic

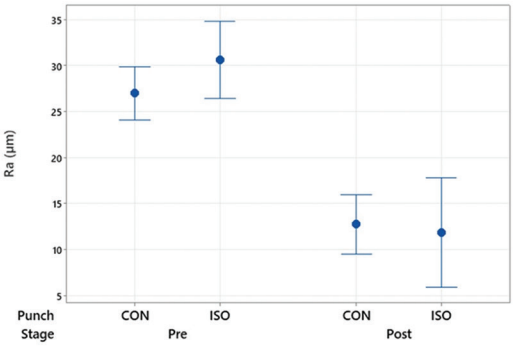

Source	DF	Adj SS	Adj MS	*F*-value	*p*-value
Stage	1	1,086.36	1,086.36	154.11	0.000
Punch	1	7.43	7.43	1.05	0.325
Stage*Punch	1	20.30	20.30	2.88	0.116
Error	12	84.59	7.05		
Total	15	1,198.67			

Figure 12. Statistical analysis of punch fillet surface roughness: Interval plot results (left) and Analysis of variance table with Tukey grouping (right) indicating significant differences among configurations
Abbreviations: Adj MS: Adjusted mean square; Adj SS: Adjusted sum of squares; CON: Concentric; DF: Degrees of freedom; ISO: Isotropic

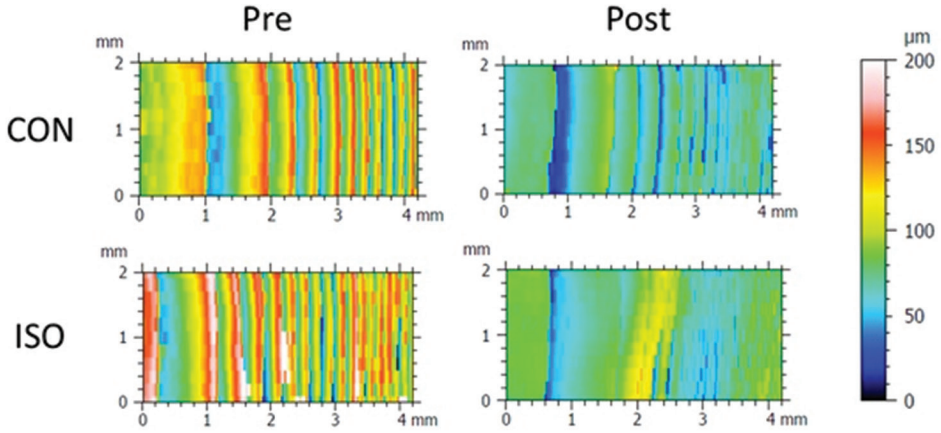

Figure 13. Three-dimensional surface scans of the punch fillet zone showing the reduction of surface roughness and stair-stepping effect after forming
Abbreviations: CON: Concentric; ISO: Isotropic

Table 3. Regression models of stress–strain relationships used as material laws in finite element model simulations

Material	Regression model
Onyx	$\sigma=5.5969+219.62\varepsilon-442.16\varepsilon^2+706.93\varepsilon^3$
Onyx with isotropic carbon fiber	$\sigma=1.826+2{,}142.5\varepsilon-13{,}560\varepsilon^2+124{,}584\varepsilon^3$
Onyx with concentric carbon fiber	$\sigma=2.2338+1{,}790.16\varepsilon-13{,}739\varepsilon^2+87{,}874\varepsilon^3$

concentric punches exhibited slightly higher peak forces—approximately 7,000 N greater than the isotropic punches at a stroke of 14 mm. The maximum force and energy values recorded during the process were approximately 110 kN and 840 Nm, respectively.

The contour maps of radial and axial displacements obtained from the simulations are shown in Figure 17. Significant differences can be observed between the two punch configurations, which help to explain the experimental results. The radial displacement maps indicate that most of the deformation occurred in the upper regions of the punches, which are composed of unreinforced polymer. Concentric punches exhibited larger radial displacements, both in terms of the affected area and absolute magnitude, which is consistent with the experimental measurements.

With respect to axial displacement, the values are plotted relative to the initial z-position of the punch. Regions remaining at −18 mm indicate no displacement, whereas higher values correspond to compression.The radial displacement maps indicate that most of the deformation occurred in the upper regions of the punches, which are composed of unreinforced polymer (Figure 17A). This behavior correlates well with the experimental measurements discussed in the previous section.

The appearance of a step-like deformation at the interface between unreinforced onyx punch and fiber-reinforced onyx further validates the material laws used as FEM input. This "stair-step" feature is visible in both punches

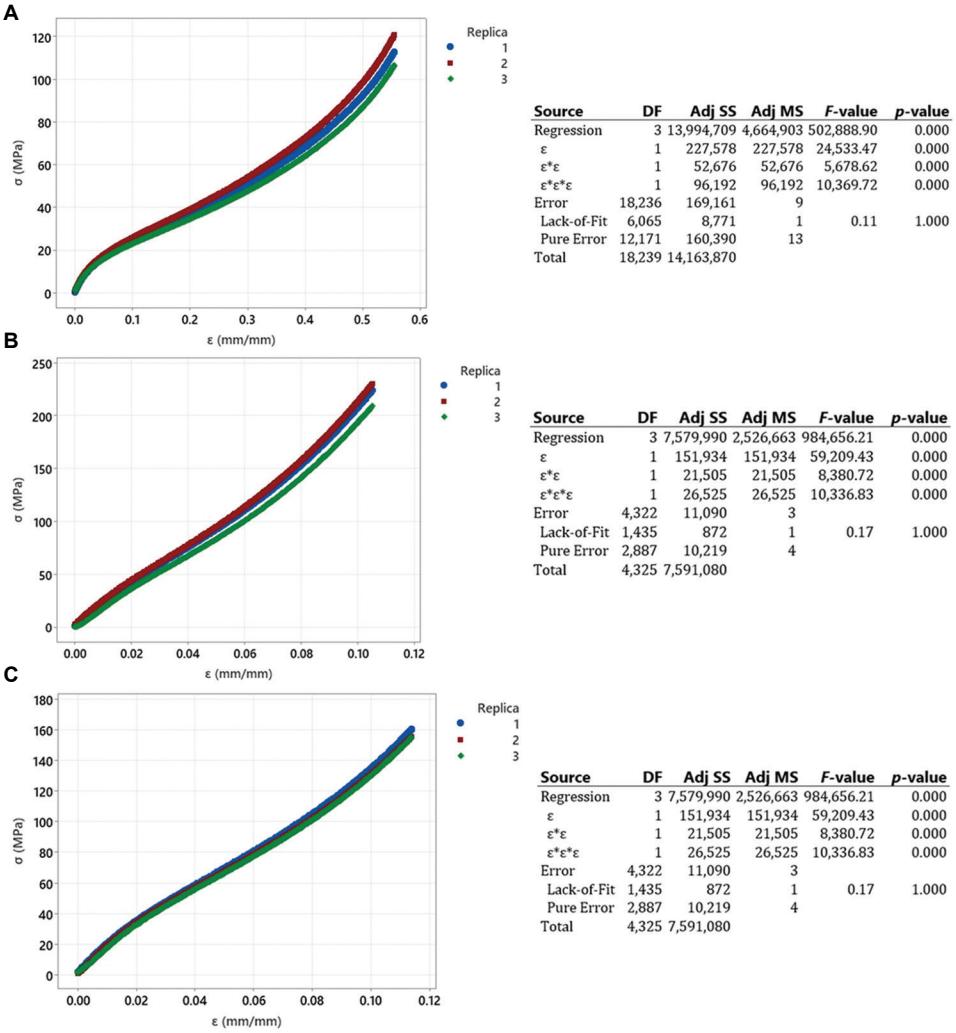

Source	DF	Adj SS	Adj MS	*F*-value	*p*-value
Regression	3	13,994,709	4,664,903	502,888.90	0.000
ε	1	227,578	227,578	24,533.47	0.000
ε*ε	1	52,676	52,676	5,678.62	0.000
ε*ε*ε	1	96,192	96,192	10,369.72	0.000
Error	18,236	169,161	9		
Lack-of-Fit	6,065	8,771	1	0.11	1.000
Pure Error	12,171	160,390	13		
Total	18,239	14,163,870			

Source	DF	Adj SS	Adj MS	*F*-value	*p*-value
Regression	3	7,579,990	2,526,663	984,656.21	0.000
ε	1	151,934	151,934	59,209.43	0.000
ε*ε	1	21,505	21,505	8,380.72	0.000
ε*ε*ε	1	26,525	26,525	10,336.83	0.000
Error	4,322	11,090	3		
Lack-of-Fit	1,435	872	1	0.17	1.000
Pure Error	2,887	10,219	4		
Total	4,325	7,591,080			

Source	DF	Adj SS	Adj MS	*F*-value	*p*-value
Regression	3	7,579,990	2,526,663	984,656.21	0.000
ε	1	151,934	151,934	59,209.43	0.000
ε*ε	1	21,505	21,505	8,380.72	0.000
ε*ε*ε	1	26,525	26,525	10,336.83	0.000
Error	4,322	11,090	3		
Lack-of-Fit	1,435	872	1	0.17	1.000
Pure Error	2,887	10,219	4		
Total	4,325	7,591,080			

Figure 14. Compression test results and Analysis of Variance of regression estimated for printed materials: (A) Onyx; (B) isotropic fiber reinforcement; and (C) concentric fiber reinforcement
Abbreviations: Adj MS: Adjusted mean square; Adj SS: Adjusted sum of squares; DF: Degrees of freedom

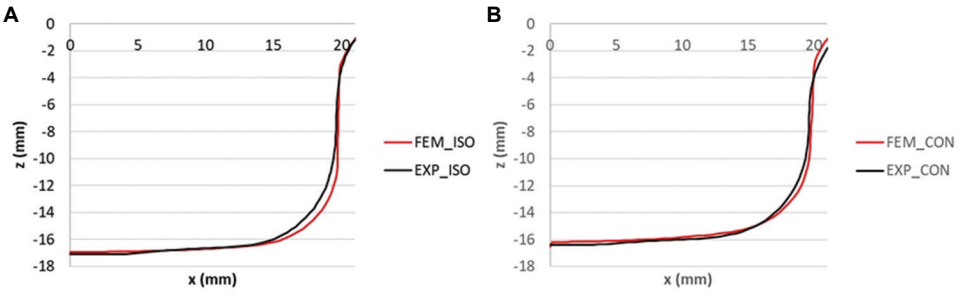

Figure 15. Validation of FEM results against experimental cup geometries for (A) ISO and (B) CON punches
Abbreviations: CON: Concentric; FEM: Finite element model; ISO: Isotropic

but is more pronounced in the isotropic configuration, as depicted in Figure 17. The same phenomenon was also confirmed experimentally, as shown in Figure 9.

These numerical insights complement the experimental observations, providing a comprehensive understanding of how fiber architecture influences tool deformation and

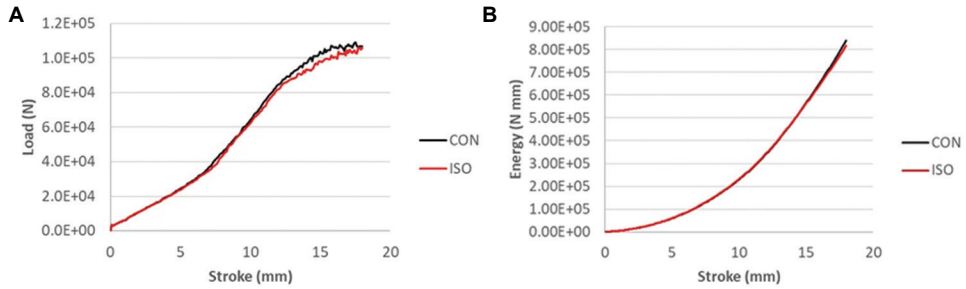

Figure 16. Finite element model predictions of (A) axial forming force and (B) forming energy as a function of punch stroke
Abbreviations: CON: Concentric; ISO: Isotropic

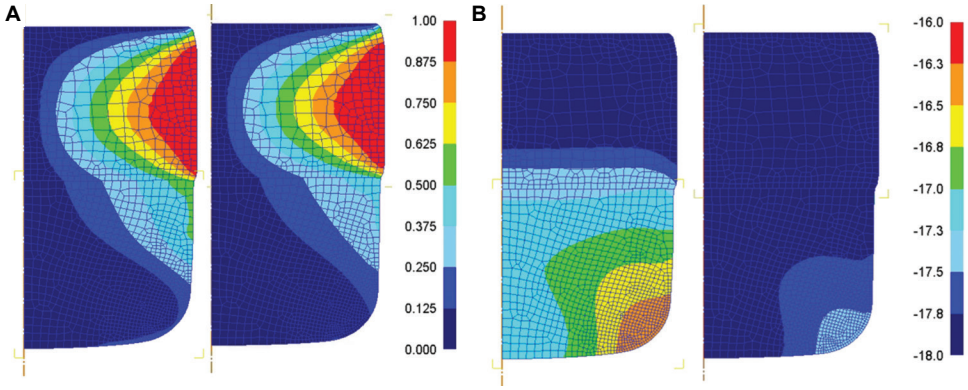

Figure 17. Finite element model contour maps of (A) radial and (B) axial displacement fields for concentric (left) and isotropic (right) punches. The green region in the concentric punch corresponds to the same location measured during the experimental campaign, represented as light blue in the isotropic punch

forming performance, thereby establishing a predictive framework for the design of additively manufactured forming tools.

5. Conclusion

The combined experimental and numerical investigation demonstrated that the fiber deposition strategy strongly influences the performance of polymer punches manufactured via CFF for deep drawing. Isotropic fiber reinforcement enabled higher drawing depths (up to 19 mm), better dimensional accuracy, and reduced punch wear compared with the concentric layout, which exhibited higher axial compression and radial deformation. Finite element simulations confirmed these experimental observations and clarified the stress transfer mechanisms within the composite punches. The study highlights the feasibility of using additively manufactured composite tools for small-scale or low-load metal forming applications, achieving significant reductions in tool weight and fabrication time. Future studies should focus on thermo-mechanical optimization and hybrid reinforcement architectures to further extend the applicability of polymer-based forming tools to industrial processes.

Acknowledgments

The authors gratefully acknowledge R. Pinti of Pinti Inox S.p.A., Sarezzo, Brescia, Italy, for assistance with the experimental work and coordinate measuring machine analyses.

Funding

None.

Conflict of interest

Luca Giorleo serves as the Editorial Board Member of the journal, but was not involved, directly or indirectly, in the editorial and peer-review process conducted for this paper. Other authors declare they have no competing interests.

Authors' contributions

Conceptualization: All authors
Data curation: Luca Giorleo
Formal analysis: Luca Giorleo
Investigation: Luca Giorleo, Davide Battini, and Andrea Avanzini
Methodology: Luca Giorleo
Software: Luca Giorleo

Supervision: Elisabetta Ceretti
Validation: Luca Giorleo
Writing – original draft: Luca Giorleo
Writing – review and editing: Luca Giorleo, Andrea Avanzini, and Davide Battini

Ethics approval and consent to participate

Not applicable.

Consent for publication

Not applicable.

Availability of data

Data are available from the corresponding author upon reasonable request.

References

1. Rosochowski A, Matuszak A. Rapid tooling: The State of the art. *J Mater Process Technol*. 2000;106(1-3):191-198.

   doi: 10.1016/S0924-0136(00)00613-0

2. Levy GN, Schindel R, Kruth JP. Rapid manufacturing and rapid tooling with layer manufacturing technologies: State of the art and future perspectives. *CIRP Ann*. 2003;52(2):589-609.

   doi: 10.1016/S0007-8506(07)60206-6

3. Merklein M, Allwood JM, Behrens BA, *et al*. Bulk forming of sheet metal. *CIRP Ann Manuf Technol*. 2012;61(2):725-745.

   doi: 10.1016/j.cirp.2012.05.007

4. Kai DA, De Lima EP, Cunico MWM, Da Costa SEG. *Additive Manufacturing: A New Paradigm for Manufacturing. In: Proceedings of the 2016 Industrial and Systems Engineering Research Conference*; 2020. p. 452-457.

5. Boparai KS, Singh R, Singh H. Development of rapid tooling using fused deposition modeling: A review. *Rapid Prototyp J*. 2016;22(2):281-299.

   doi: 10.1108/RPJ-04-2014-0048

6. Hussin RB, Sharif SB, Abd Rahim SZB, *et al*. The potential of metal epoxy composite as hybrid mold inserts in rapid tooling application: A review. *Rapid Prototyp J*. 2021;27(6):1069-1100.

   doi: 10.1108/RPJ-01-2020-0025

7. Vaghela JR, Valaki JB, Thanki SJ, Pandey AB. Sustainability analysis of rapid tooling-based investment casting: A comprehensive review. *Smart Sustain Manuf Syst*. 2023;7(1):54-81.

   doi: 10.1520/SSMS20220029

8. Gülçür M, Rich A, Griffiths O, Wilson P, Williams M, Gibbons G. Rapid tooling: Comparative analysis of mechanical properties and energy efficiency in micro-injection mouldings using polymer and metal moulds. *Manuf Lett*. 2025;45:31-35.

   doi: 10.1016/j.mfglet.2025.06.204

9. Frohn-Sörensen P, Geueke M, Engel B, *et al*. Design for 3D printed tools: Mechanical material properties for direct polymer additive tooling. *Polymers*. 2022;14(9):1694.

   doi: 10.3390/polym14091694

10. Pelegatti M, Benasciutti D, De Bona F, *et al*. On the factors influencing the elastoplastic cyclic response and low cycle fatigue failure of AISI 316L steel produced by laser-powder bed fusion. *Int J Fatigue*. 2022;165:107224.

    doi: 10.1016/j.ijfatigue.2022.107224

11. Kumar S, Singh AK. FDM modeled polymer tooling for plastic injection molding. *Int J Adv Mater Sci Eng*. 2018;7(1):9-19.

    doi: 10.14810/ijamse.2018.7102

12. Giolu C, Pupăză C, Amza CG. Exploring polymer-based additive manufacturing for cost-effective stamping devices: A feasibility study with finite element analysis. *Polymers (Basel)*. 2024;16(13):1894.

    doi: 10.3390/polym16131894

13. Giorleo L, Deniz KI. Topology optimization of polymer-based bending tools manufactured via additive technology: Numerical and experimental validation. *J Manuf Mater Process*. 2025;9(9):310.

    doi: 10.3390/jmmp9090310

14. Salifu S, Desai D, Ogunbiyi O, Mwale K. Recent development in the additive manufacturing of polymer-based composites for automotive structures: A review. *Int J Adv Manuf Technol*. 2022;119(11):6877-6891.

    doi: 10.1007/s00170-021-08569-z

15. Pinto M, Santos AD, Teixeira P, Bolt PJ. Study on the usability and robustness of polymer and wood materials for tooling in sheet metal forming. *J Mater Process Technol*. 2008;202 (1-3):47-53.

    doi: 10.1016/j.jmatprotec.2007.08.082

16. Liewald M, De Souza JHC. New developments on the use of polymeric materials in sheet metal forming. *Prod Eng*. 2008;2(1):63-72.

    doi: 10.1007/s11740-008-0077-5

17. Giorleo L, Ceretti E. Aluminium deep drawing with additive manufacturing polymer punches: Performance analysis in small batch production. *Int J Adv Manuf Technol*. 2023;128(5):2175-2185.

    doi: 10.1007/s00170-023-12066-w

18. Gaudenzi G, Giorleo L, Ceretti E. Performance analysis of composite and steel deep drawing tools combination. Int J *Adv Manuf Technol*. 2025;136(2):581-600.

    doi: 10.1007/s00170-024-14875-z

19. Schuh G, Bergweiler G, Bickendorf P, Fiedler F, Colag C. Sheet metal forming using additively manufactured polymer tools. *Procedia CIRP*. 2020;93:20-25.

doi: 10.1016/j.procir.2020.04.013

20. Geueke M, Frohn-Sörensen P, Reuter J, Padavu N, Reinicke T, Engel B. Structural optimization of additively manufactured polymer tools for flexible sheet metal forming. P*rocedia CIRP*. 2021;104:1345-1350.

doi: 10.1016/j.procir.2021.11.226

21. Pelin G, Sonmez M, Pelin CE. The use of additive manufacturing techniques in the development of polymeric molds: A review. *Polymers (Basel)*. 2024;16(8):1055.

doi: 10.3390/polym16081055

22. Sathishkumar N, Arumaikkannu G, Hariharan K. Design of a direct rapid tool for hydroforming of metal bellows using additively manufactured polymer die. *Int J Interact Des Manuf*. 2024;18(7):4941-4962.

doi: 10.1007/s12008-024-01821-2

23. Giorleo L, Ceretti E. Deep drawing punches produced using fused filament fabrication technology: Performance evaluation. *J Manuf Process*. 2022;84:1-9.

doi: 10.1016/j.jmapro.2022.09.054

24. Burnett C, Graninger G, Eren Z, Falzon BG, Kazancı Z. Tensile performance of carbon fibre-reinforced 3D-printed polymers: Effect of printing parameters. *Eng Fail Anal*. 2025;175:109577.

doi: 10.1016/j.engfailanal.2025.109577

25. Available from: https://markforged.com/materials/plastics/onyx visited 24/11/25

26. Available from: https://www.matweb.com/visited 24/11/25

27. Unal H, Mimaroglu A. Friction and wear performance of polyamide 6 and graphite and wax polyamide 6 composites under dry sliding conditions. *Wear*. 2012;289:132-137.

doi: 10.1016/j.wear.2012.04.004

28. Meng H, Sui GX, Xie GY, Yang R. Friction and wear behavior of carbon nanotubes reinforced polyamide 6 composites under dry sliding and water-lubricated condition. *Compos Sci Technol*. 2009;69(5):606-611.

doi: 10.1016/j.compscitech.2008.12.004